

Mitigating early-age cracking in thin UHPFRC precast concrete products using shrinkage-reducing admixtures

Doo-Yeol Yoo, Nemkumar Banthia, and Young-Soo Yoon

- This study investigates the effects of different shrinkage-reducing admixture amounts and cover depths on the shrinkage and surface-cracking behavior of ultra-high-performance fiber-reinforced concrete (UHPFRC) slabs.
- Slabs with shrinkage-reducing admixture exhibited better behavior with regard to the decrease of shrinkage, maximum evaporation rate, and maximum surface-crack width. A larger cover depth was favorable because it caused a lower degree of restraint, leading to a lower cracking potential and a higher surface-cracking resistance.
- The minimum required cover depth of the UHPFRC slab is suggested to be 1.3 times larger than the diameter of the upper steel reinforcing bar in order to prevent surface cracking.

Concrete has been widely used for construction because of its superior mechanical strength, durability, and economical efficiency compared with other construction materials. However, concrete also has inherent drawbacks, such as heavy density, enlargement of self-load, low tensile strength, low ductility, and a low strength-to-weight ratio. For decades, numerous studies have been conducted to find ways to improve concrete's strength and ductility. Ultra-high-performance fiber-reinforced concrete (UHPFRC) has recently been considered one of the most promising new materials to overcome the intrinsic drawbacks of previous concretes because of its excellent strength (compressive strength > 150 MPa [22 ksi] and tensile strength > 8 MPa [1 ksi]), ductility, fatigue performance, and durability.¹ These excellent properties of UHPFRC are achieved by reducing the water-to-binder ratio, by incorporating high-fineness admixtures based on the packing theory, and by including high-volume fractions of short steel fibers. In particular, UHPFRC has been attractive for precast concrete thin-plate structures, such as slabs, thin walls, roofs, architectural panels, and bridge-deck joints, due to its unique strain-hardening response with multiple small cracks and superb bond strength.²⁻⁵

Because of its low water-to-binder ratio and use of high-fineness admixtures, UHPFRC exhibits extremely high autogenous shrinkage.⁶ Furthermore, because thin-plate

Table 1. Mixture proportions

Specimen	Relative weight to cement ratios						Steel fiber V_f , %	Flow, mm	
	Cement	Water	Silica fume	Silica sand	Silica flour	SP			SRA
UH-S0	1.00	0.25	0.25	1.10	0.30	0.018	0.00	235	
UH-S1							0.01		245
UH-S2							0.02		

Note: SP = superplasticizer; SRA = shrinkage-reducing admixture; UH = ultra-high-performance fiber-reinforced concrete; V_f = volume fraction of fiber. 1 mm = 0.0394 in.

structures and bridge-deck joints made of UHPFRC have small cross-sectional areas with internal steel reinforcement, they are weak and result in cracking due to the restraint of shrinkage and settlement. The Japan Society of Civil Engineers⁷ recommended that deformed steel reinforcement be used carefully in structures made of UHPFRC because of the high possibility of shrinkage cracking. Many researchers have also performed restrained-shrinkage tests for UHPFRC elements.^{6,8-11} Yoo et al.¹⁰ used a modified ring test to evaluate various parameters of the restrained shrinkage behavior of UHPFRC, such as residual stress, degree of restraint, and cracking potential. In their results, approximately 39% to 65% of elastic stresses were relaxed by the sustained restraint load. Thus, stress relaxation (or creep) must be considered for evaluating restrained shrinkage behaviors.

Park et al.⁹ and Yoo et al.¹¹ verified the effectiveness of the combined use of 1% shrinkage-reducing admixture (SRA) and 7.5% expansive admixture on the improvement of restrained shrinkage cracking resistance of UHPFRC using the drying shrinkage-crack test in accordance with KS F 2595¹² and the full-scale restrained slab test. Habel et al.⁸ experimentally verified that early-age creep deformation of UHPFRC represents 65% of autogenous shrinkage in restrained conditions. Likewise, most of the previous studies have focused on estimating the shrinkage and cracking behaviors of UHPFRC restrained by external forms, whereas only a limited number of studies⁶ are available on the restrained shrinkage behavior of UHPFRC elicited by internal reinforcement.

Surface cracking, which typically occurs parallel to the longitudinal direction of the upper reinforcement, is mainly influenced by settling and plastic shrinkage and leads to the decrease of durability in concrete structures. Thus, to prevent surface cracking, sufficient cover depth is required. Alternatively, an SRA can be added because it reduces the drying and plastic shrinkage at an early age (and permeation of hazardous materials) by increasing the pore solution's viscosity. It also reduces autogenous shrinkage by diminishing the surface tension of the pore solution by approximately 50% or more in hydrated cement paste.¹³ Specifically, the determination of minimum cover depth is important for the application of UHPFRC

to precast concrete thin-plate structures in order to prevent surface cracking. However, no published studies exist on the surface-cracking behavior of UHPFRC slabs related to cover depth.

Accordingly, in this study, a series of surface-cracking tests for UHPFRC slabs with steel reinforcement were conducted in order to suggest a minimum cover depth to prevent surface cracking for three different SRA dosages (0%, 1%, and 2%) and cover depths (5, 10, and 20 mm [0.2, 0.4, and 0.8 in.]). The effect of the SRA dosage on the properties of fresh concrete, such as setting and water evaporation rate, were analyzed. The restrained shrinkage performance of UHPFRC slabs by internal steel reinforcement was also investigated for three different SRA dosages and cover depths.

Test program

Materials and specimen preparation


Table 1 gives the mixture proportions used in this study. ASTM Type I portland cement and silica fume were used as cementitious materials, and **Table 2** summarizes their chemical compositions and physical properties. The water-to-binder ratio used was 0.2. Silica sand with a grain size below 0.5 mm (0.02 in.) was used as the fine aggregate,

Table 2. Chemical compositions and physical properties of cementitious materials

Composition	Cement	Silica fume
CaO, % mass	61.33	0.38
Al ₂ O ₃ , % mass	6.40	0.25
SiO ₂ , % mass	21.01	96.00
Fe ₂ O ₃ , % mass	3.12	0.12
MgO, % mass	3.02	0.10
SO ₃ , % mass	2.30	n/a
Specific surface, cm ² /g	3413	200,000
Density, g/cm ³	3.15	2.10

Note: n/a = not applicable. 1 cm = 0.394 in. 1 g = 0.0353 oz.

Table 3. Properties of steel fibers

d_f , mm	L_f , mm	Aspect ratio L_f/d_f	Density, g/cm ³	f_b , MPa	E_b , GPa	Image
0.2	13.0	65.0	7.9	2500.0	200.0	

Note: d_f = diameter of fiber; E_b = elastic modulus of fiber; f_b = tensile strength of fiber; L_f = length of fiber. 1 mm = 0.0394 in.; 1 cm = 0.394 in.; 1 g = 0.0353 oz; 1 MPa = 0.145 ksi; 1 GPa = 145 ksi.

and silica flour with a 2 μ m (0.00008 in.) diameter and composition of 98% SiO₂ was used as the filling powder. Coarse aggregate was excluded from the mixture to improve its homogeneity. To provide suitable workability, a high-range water-reducing admixture (HRWRA), polycarboxylate superplasticizer, was added. Two percent (by volume of the total mixture) of smooth steel fibers with a length of 13 mm (0.51 in.) and a diameter of 0.2 mm (0.008 in.) were incorporated to improve tensile strength and ductility. **Table 3** lists the properties of the steel fibers. To evaluate the effect of SRA on the properties of fresh concrete and on shrinkage, a glycol-based powder-type SRA was added at three different dosage rates (0%, 1%, and 2% by weight), leading to three series of test specimens. The letters UH and S indicate the UHPFRC and the SRA, while the numeral indicates the dosage of SRA. For instance, specimen UH-S1 refers to the UHPFRC that includes 1% of SRA (by weight).

Because UHPFRC has a low water-to-binder ratio of 0.2 and high-fineness aggregates without coarse aggregate, the mixing sequence is different from that used for ordinary concrete as follows:

1. Cement, silica fume, silica sand, silica flour, and SRA were mixed for 10 minutes.
2. Water mixed with 1.8% HRWRA was poured into the dry materials and mixed for another 10 minutes.
3. Once the mixture showed adequate fluidity and viscosity, 2% (by volume) of steel fibers were dispersed and mixed for another 5 minutes.

All specimens were cured at a temperature of 23°C (73.4°F) and a humidity of 60% \pm 5% during testing.

Test setup and procedure

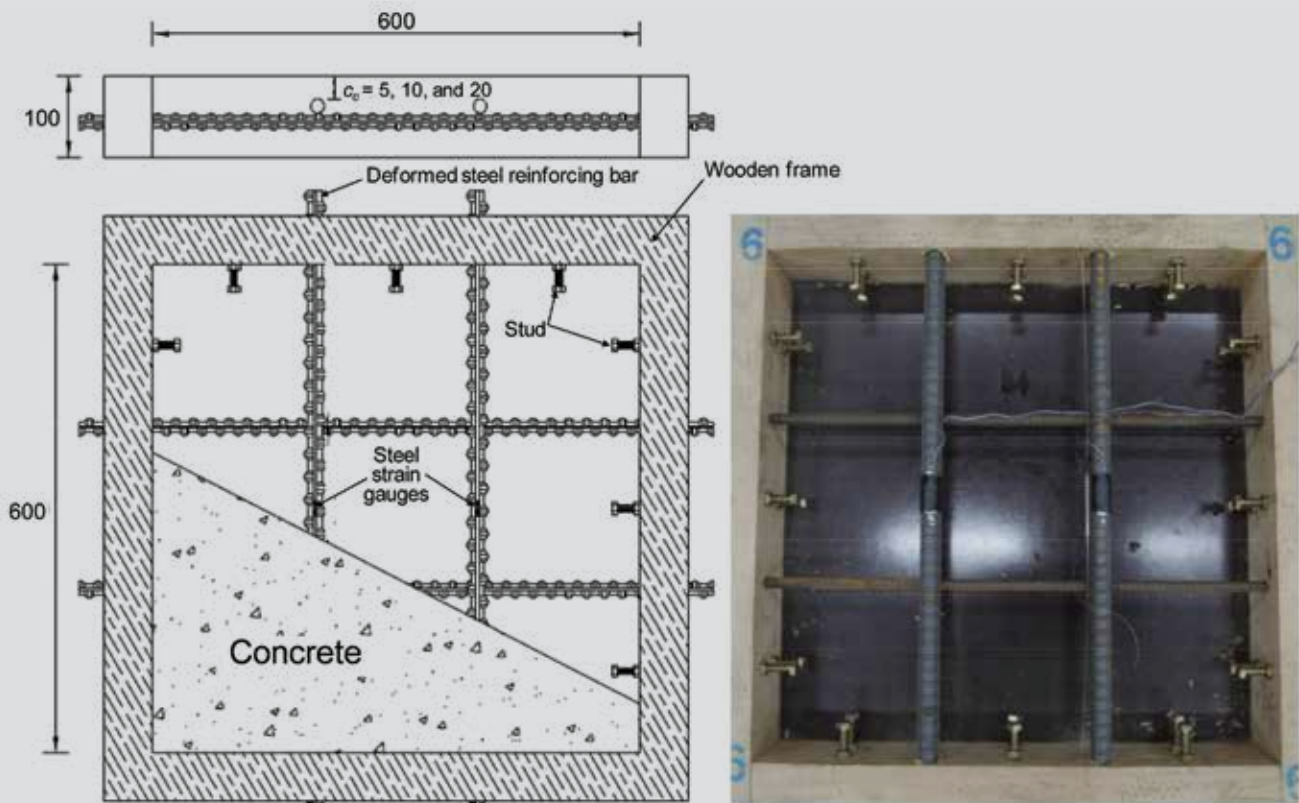
Properties of fresh concrete (fluidity, setting, and evaporation rate) A flow-table test was performed as per ASTM C1437¹⁴ to estimate fluidity. The average flows were calculated by averaging the maximum flow diameter and the perpendicular diameter to the maximum flow diameter (Table 1). The lowest flow of 235 mm (9.25

in.) was obtained for UH-S0, and fluidity slightly increased with the addition of the SRA.^{15,16}

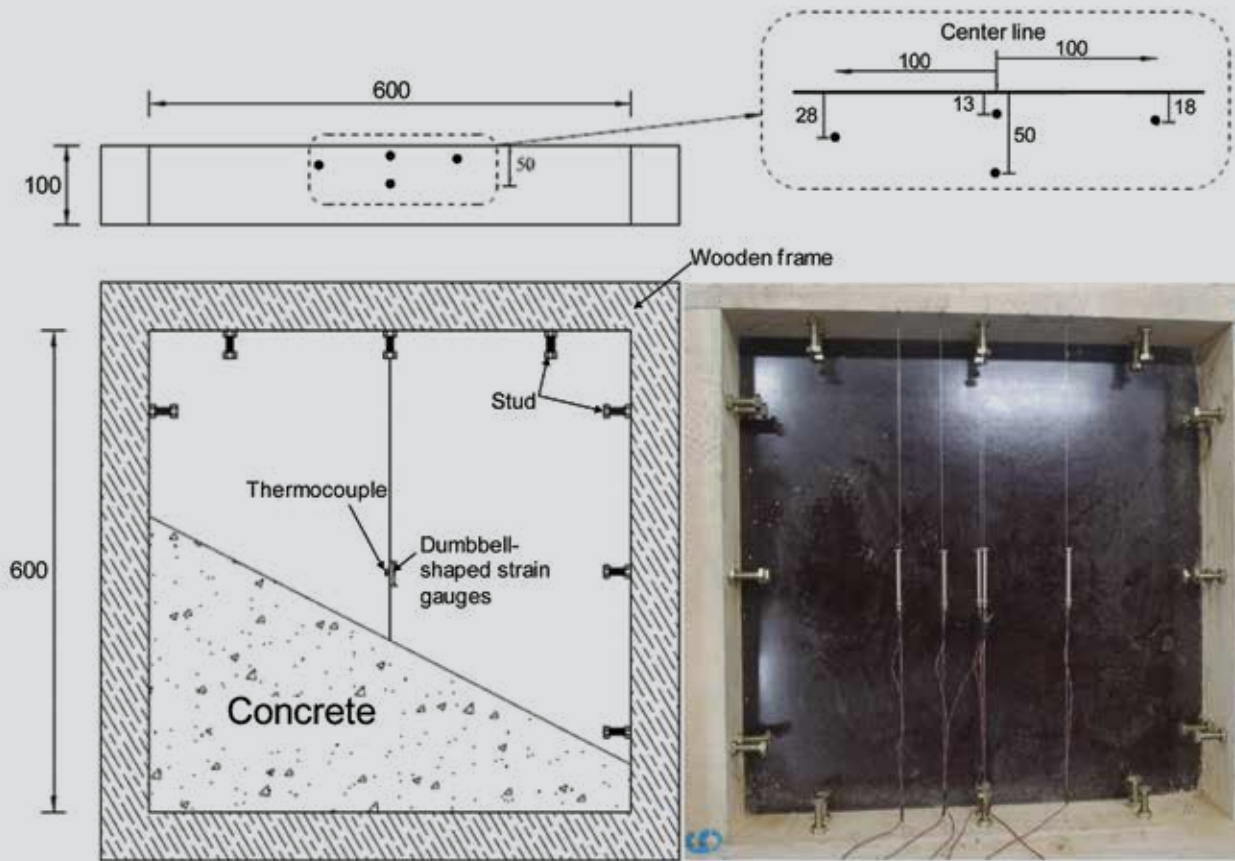
The setting properties of UHPFRC without fibers were investigated by the penetration-resistance test according to ASTM C403.¹⁷ Because UHPFRC has a low water-to-binder ratio, the rate of water evaporation on the surface is larger than the rate of bleeding. Thus, the surface dries rapidly even when it is only briefly exposed to the atmosphere. This causes overestimation of the penetration resistance. For this reason, Yoo et al.¹⁸ suggested a method to prevent water evaporation during the penetration-resistance test by using liquid paraffin oil on the surface of the mortar. Therefore, in this study, cylindrical plastic molds were used with dimensions of 150 \times 160 mm (5.9 \times 6.3 in.), and the mortar was filled until the surface was 10 mm (0.4 in.) below the top edge of the mold. Thereafter, liquid paraffin oil was poured onto the surface of the mortar to prevent surface drying. The needle penetrated the mortar at a depth of 25 \pm 2 mm (0.98 \pm 0.08 in.) in 10 seconds, and the clear-distance rule for needle impressions was followed.

To investigate the effect of the SRA dosage on the evaporation rate of water, mass loss was measured. To achieve this, two containers with an exposed-surface dimension of 200 \times 145 mm (7.8 \times 5.7 in.) were used for each variable, similar to the tests by Pelisser et al.¹⁹ The mass loss of the specimens was immediately measured from concrete casting using an electronic scale with a minimum scale of 0.01 g (0.035 oz) until a convergence value was reached.

Surface-cracking behavior of UHPFRC slabs To investigate the effects of SRA dosage and cover depth on the surface-cracking resistance of UHPFRC slabs, three different SRA dosage rates (0%, 1%, and 2%) and three different cover depths (5, 10, and 20 mm [0.2, 0.4, and 0.8 in.]) were considered. **Figure 1** shows the test setup. Prismatic specimens were used with dimensions of 600 \times 600 mm (24 \times 24 in.) and a height of 100 mm (4 in.). Because of the uncertainty in material performance (that is, the tensile performance of UHPFRC is strongly influenced by the fiber orientation), steel reinforcing bars have been included in thin UHPFRC slabs in Korea. Therefore, to account for uncertain tensile performance and to provide



Slabs with steel reinforcing bars



Slab without steel reinforcing bar

Figure 1. Shrinkage and surface-cracking-test setup for ultra-high-performance fiber-reinforced concrete slabs. Note: all measurements are in millimeters. c_c = concrete cover depth. 1 mm = 0.0394 in.

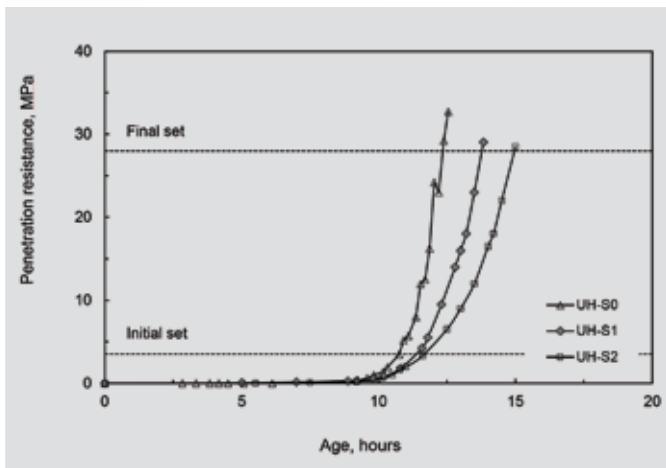


Figure 2. Penetration-resistance-test results. Note: 1 MPa = 0.145 ksi.

uniform boundary conditions for all test series, D16 (diameter of 15.9 mm [0.626 in.]) and D13 (diameter of 12.7 mm [0.50 in.]) steel bars were used as upper and lower reinforcement, respectively. To better represent in-place conditions, the side surfaces of the slabs were restrained by steel studs to account for the restraining effect of the surrounding contiguous element. In addition, wood was used as an external form to prevent thermal deformation. Two strain gauges were attached to the center of the upper steel reinforcing bars to measure strain. Furthermore, it was assumed that the bond slip between reinforcement and concrete by shrinkage would be negligible, based on a previous study.²⁰

To quantitatively estimate the restraining effect of steel reinforcement on shrinkage, prismatic specimens identical in size to the surface-cracking-test specimens were fabricated without reinforcement. Studs were also used at the external frame to mimic the restraining effect of the surrounding

Table 4. Setting properties

Specimen	Initial set, hr	Final set, hr
UH-S0	10.8	12.3
UH-S1	11.4	13.8
UH-S2	11.7	15.0

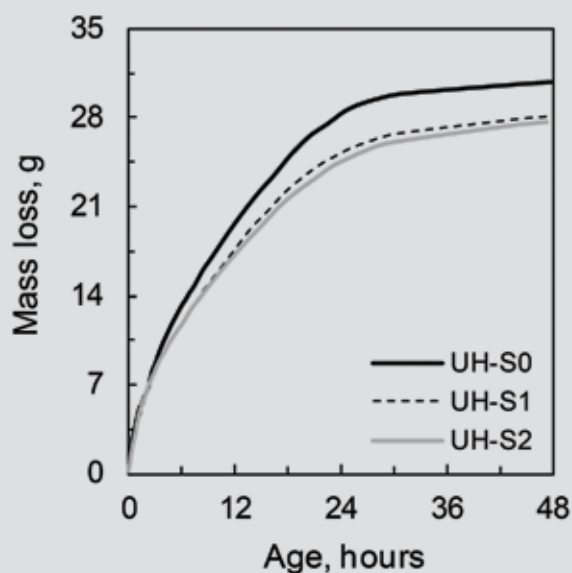
contiguous element. To measure the strain and temperature at each location of the steel reinforcing bars, four dumb-bell-shaped strain gauges with nearly zero stiffness and a coefficient of thermal expansion of $11 \mu\epsilon/^\circ\text{C}$ ($6 \mu\epsilon/^\circ\text{F}$) and four thermocouples were embedded (Fig. 1). The strains and temperatures were immediately measured during the concrete casting.

Test results and discussion

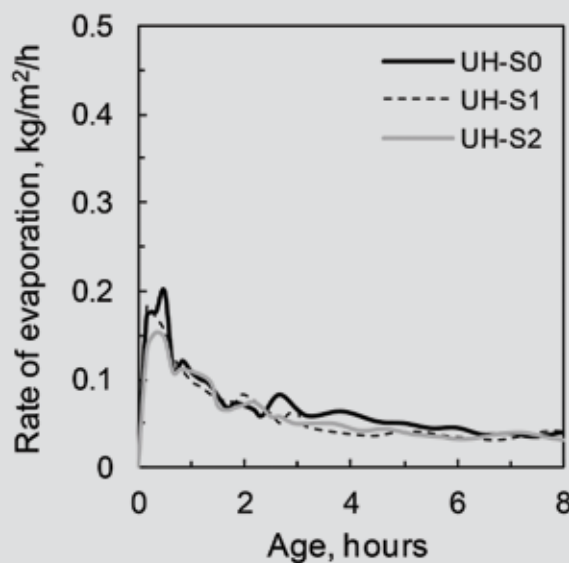
Properties of fresh concrete

Figure 2 shows the development of penetration resistance for UHPFRC mortar related to SRA dosage. The increase of penetration resistance was delayed as a function of the increase of SRA dosage. Thus, the times for the initial and final sets were delayed with increasing SRA dosage (**Table 4**). This is because the reduction of water surface tension by the addition of SRA decreases the interparticle force, thereby attracting the flocculated binder phase and thus retarding setting times. This is consistent with the findings of Brooks et al.²¹

Figure 3 shows the average values of mass loss and evaporation rate. Regardless of the SRA dosage, mass loss from water evaporation steadily increased with age, yet the increase rate of mass loss reduced with age. The maximum



Mass loss



Rate of evaporation

Figure 3. Effect of shrinkage-reducing admixture dosage on water evaporation. Note: 1 m = 3.28 ft; 1 g = 0.0353 oz; 1 kg = 2.20 lb.

mass loss and evaporation rate decreased with the increase in SRA dosage. This is in accordance with the findings of Mora-Ruacho et al.²² and attributed to the increase of the pore solution's viscosity.¹³ Bentz²³ reported that the viscosity of a 10% SRA solution in distilled water is approximately 50% greater than that of pure distilled water, which causes a slower internal flow rate. The maximum rate of evaporation for specimen UH-S0 was found to be 0.20 kg/m²/hr (0.04 lb/ft²/hr), approximately 10% and 30% greater than that of specimens UH-S1 and UH-S2, respectively. This value is also much less than those of conventional normal- and high-strength concretes²² owing to the extremely densified microstructure of UHPFRC. The evaporation rate reduced with age and converged to a stable value after reaching the peak value.

Restrained shrinkage behavior of UHPFRC slabs by internal steel reinforcement

No shrinkage stress occurs in fresh concrete because of its nearly zero stiffness. Thus, to estimate the net shrinkage that causes cracking in concrete, the strains generated within the period during which concrete was fresh were excluded. Yoo et al.⁶ reported that shrinkage stress in concrete first develops when the internal steel reinforcement starts to deform by shrinkage, and this point is close to the deviation point between the strain and the internal temperature. In this study, therefore, the zero point of shrinkage measurement, which is called time-zero, is defined by the deviation point of strain and temperature for analyzing restrained shrinkage behavior by internal steel reinforcement.

Figure 4 shows the shrinkage behavior of the UHPFRC slabs without steel reinforcement by SRA dosage and cover depth. At the beginning (before time-zero), the measured strains slightly increased due to the decrease in the temperature of the concrete. After time-zero, the strains measured by the embedded strain gauge rapidly increased because both the shrinkage and elastic modulus of UHPFRC started to increase. As the depth from the exposed surface decreased, the strains increased due to the increase in water evaporation. Approximately one day after the casting of the concrete, the increased rate of shrinkage strain suddenly decreased. This is because the chemical shrinkage and volume contraction from the negative pressure in the internal voids were self-restrained by the hardening of the concrete.⁹

The shrinkage strain of UHPFRC after 30 days was reduced by adding the SRA, and the amount of decrease in shrinkage increased with the increase of SRA dosage (**Fig. 5**). For instance, the 30-day shrinkage strain of specimen UH-S0 at a depth of 13 mm (0.51 in.) was found to be $-862 \mu\epsilon$, approximately 5% and 12% higher than those of specimens UH-S1 and UH-S2, respectively. In addition, the shrinkage strain significantly decreased with an increase in

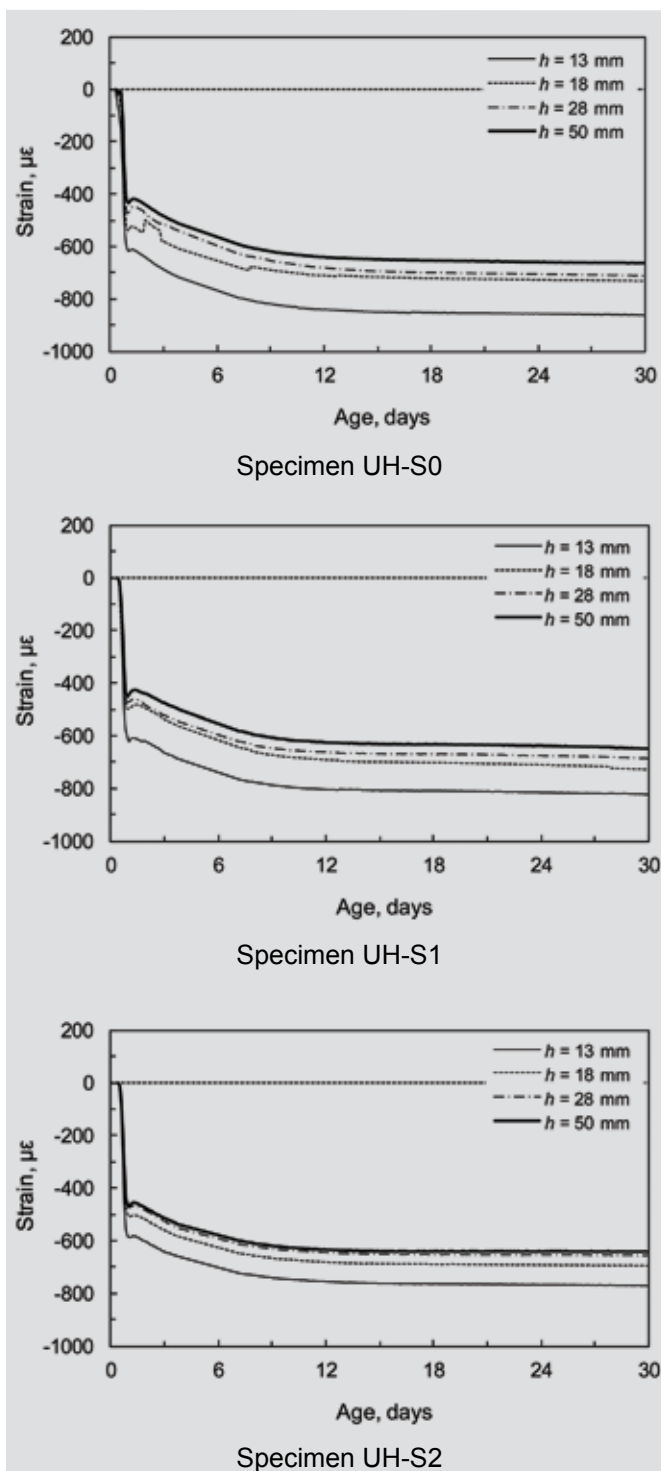


Figure 4. Shrinkage strains of ultra-high-performance fiber-reinforced concrete slabs without steel reinforcement. Note: h = depth of slab. 1 mm = 0.0394 in.

the depth from the exposed surface up to 18 mm (0.71 in.), and a more gradual shrinkage-strain decrease was observed at greater depths.

Figure 6 shows the internal temperature behaviors at a depth of 50 mm (2 in.). Similar results were obtained at different depths. A slightly higher maximum temperature (by 31.8°C [89.2°F]) was obtained for specimen UH-S0,

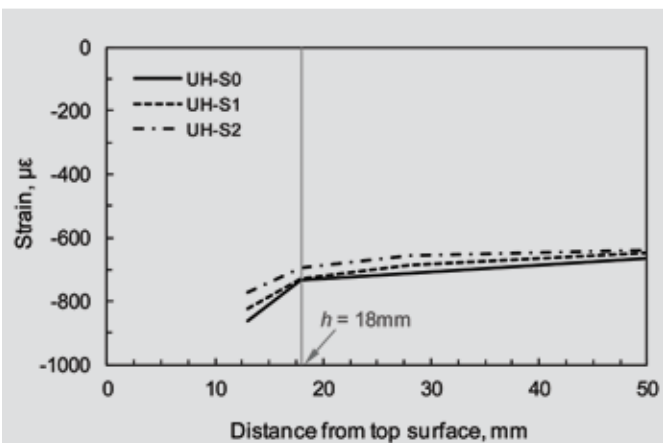


Figure 5. Effects of shrinkage-reducing admixture dosage and cover depth on 30-day shrinkage strains of ultra-high-performance fiber-reinforced concrete slabs without steel reinforcement. Note: 1 mm = 0.0394 in.

approximately 5% higher than those of specimens UH-S1 and UH-S2. However, because the difference in temperature behavior according to SRA dosage was small, it can be concluded that the effect of SRA on the internal temperature behavior of UHPFRC is insignificant, consistent with the findings of Saliba et al.¹⁵

Figure 7 exhibits actual residual strains in steel reinforcement according to cover depth and SRA dosage. Actual residual strain indicates the strain measured in the steel reinforcement with consideration of creep. The shape of strain development in the steel reinforcement was similar to that in the UHPFRC slab without steel reinforcement in Fig. 4; however, much smaller values were obtained (**Fig. 8**). In particular, early-age strains in the steel reinforcement (at nearly one day) were almost three times smaller than the strains in slabs without steel reinforcement. This is because of the low elastic modulus of concrete at early age. Residual strain is influenced by both the shrinkage and elastic modulus of concrete. Therefore, although the shrinkage strains in slabs without steel reinforcement steeply increased from time-zero, small residual strains in steel reinforcement were obtained at early age. After nearly one day, strains in the steel reinforce-

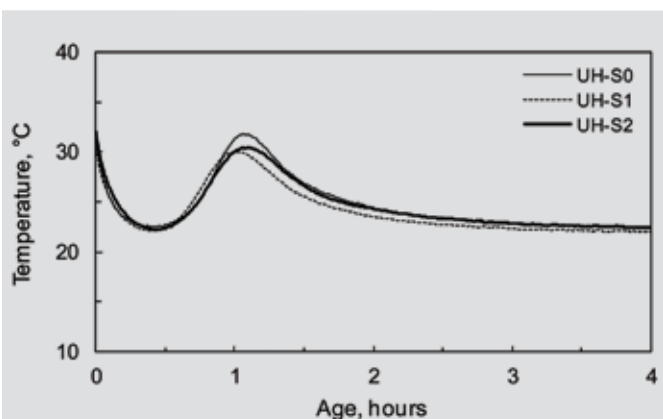
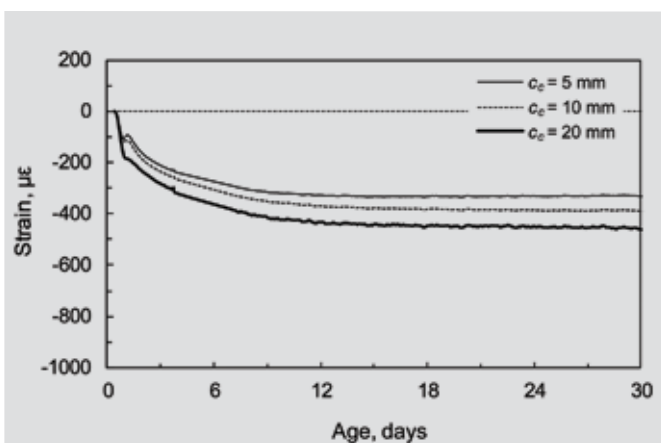
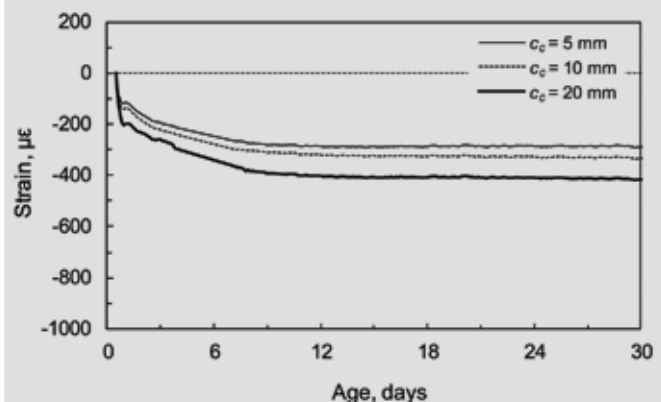


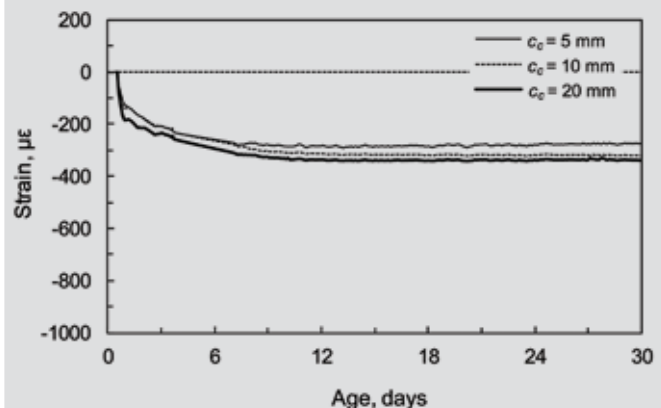
Figure 6. Effect of shrinkage-reducing admixture content on internal temperature at height of 50 mm. Note: 1 mm = 0.0394 in.; $^{\circ}\text{F} = 1.8(^{\circ}\text{C}) + 32$.



Specimen UH-S0



Specimen UH-S1



Specimen UH-S2

Figure 7. Strains measured in steel reinforcing bars with different cover depths. Note: c_c = concrete cover depth. 1 mm = 0.0394 in.

ment gradually increased and thus the shrinkage strain in the slabs with steel reinforcement behaved similarly to the shrinkage strain of slabs without steel reinforcement.

Figure 9 shows the 30-day residual strains and stresses measured in the steel reinforcement. Both the residual strain and stress increased with the cover depth from the top surface. This is mainly caused by the fact that, although the shrinkage strain decreased with depth, more

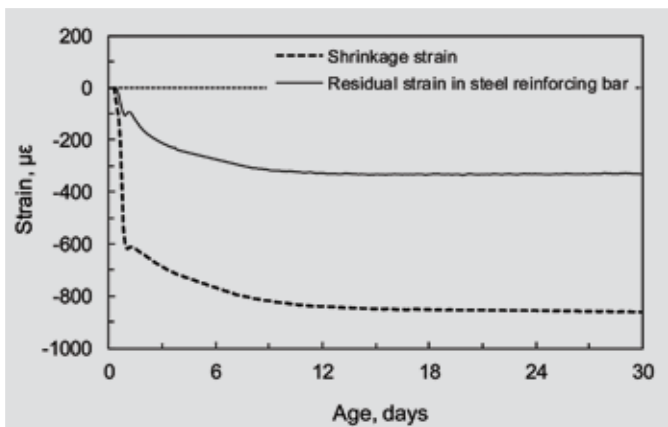


Figure 8. Comparison of shrinkage strain for ultra-high-performance fiber-reinforced concrete slab without steel reinforcement at a height of 13 mm (0.5 in.) and residual strain in steel reinforcement at cover depth of 5 mm (0.2 in.) (UH-S0).

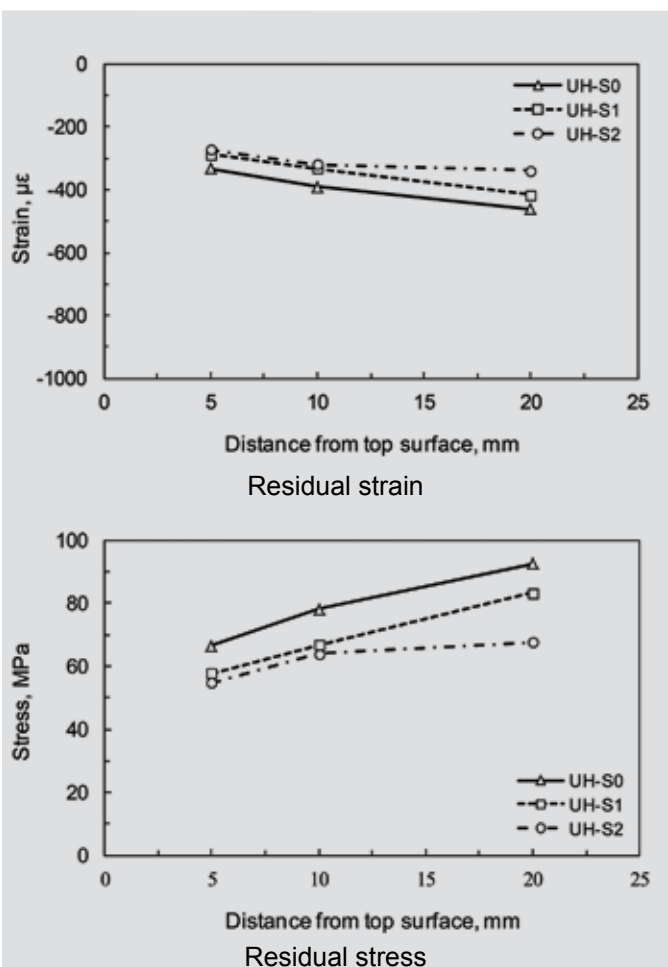


Figure 9. Effects of shrinkage-reducing admixture content and cover depth on residual strain and stress in steel reinforcing bar at 30 days. Note: 1 mm = 0.0394 in.; 1 MPa = 0.145 ksi.

force from the restraint of the shrinkage was transferred from the concrete to the steel reinforcement with the increase of cover depth by equilibrium, which leads to an increased area of the surrounding concrete. The increase of the residual strain with the increase in the ratio between

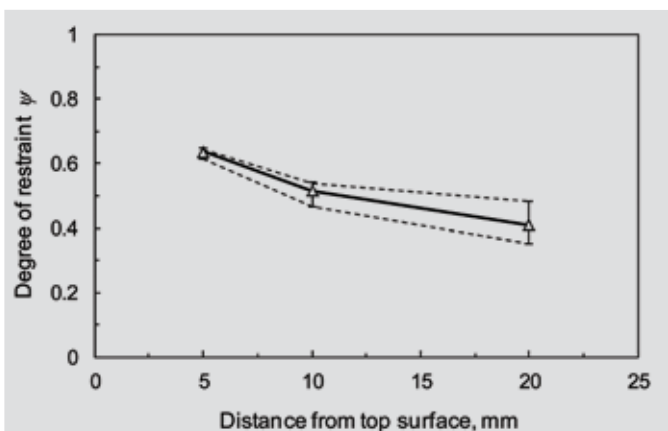


Figure 10. Average degree of restraint according to cover depth at 30 days. Note: 1 mm = 0.0394 in.

the areas of the concrete and the steel reinforcement was reported in a previous study.²⁴ Smaller residual stresses were obtained at greater SRA dosage rates and at lesser cover depths. Specimen UH-S0 exhibited the largest compressive stresses, ranging from 66.5 to 92.5 MPa (9.64 to 13.4 ksi), approximately 11% to 17% and 22% to 37% larger than those of specimens UH-S1 and UH-S2, respectively.

To quantitatively investigate the degree of restraint according to cover depth, Eq. (1) is used for the ratio between the residual strain and the shrinkage of concrete without reinforcement:

$$\psi = 1 - \frac{\epsilon_s}{\epsilon_{sh}} \quad (1)$$

where

ψ = degree of restraint

ϵ_s = strain in steel reinforcement

ϵ_{sh} = shrinkage strain of concrete without reinforcement

Because the degree of restraint is insignificantly affected by SRA dosage,²⁵ only the effect of the cover depth on the average degree of restraint for all test specimens at 30 days was investigated (Fig. 10). The degree of restraint decreased as cover depth increased for all test specimens. In general, a higher degree of restraint results in a greater cracking potential in concrete.²⁶ Therefore, it is noted that a shallow cover depth is unfavorable because it increases the cracking potential of UHPFRC slabs by the restraint of shrinkage.

Surface-cracking behavior of UHPFRC slabs

Figure 11 shows the surface-cracking behaviors of

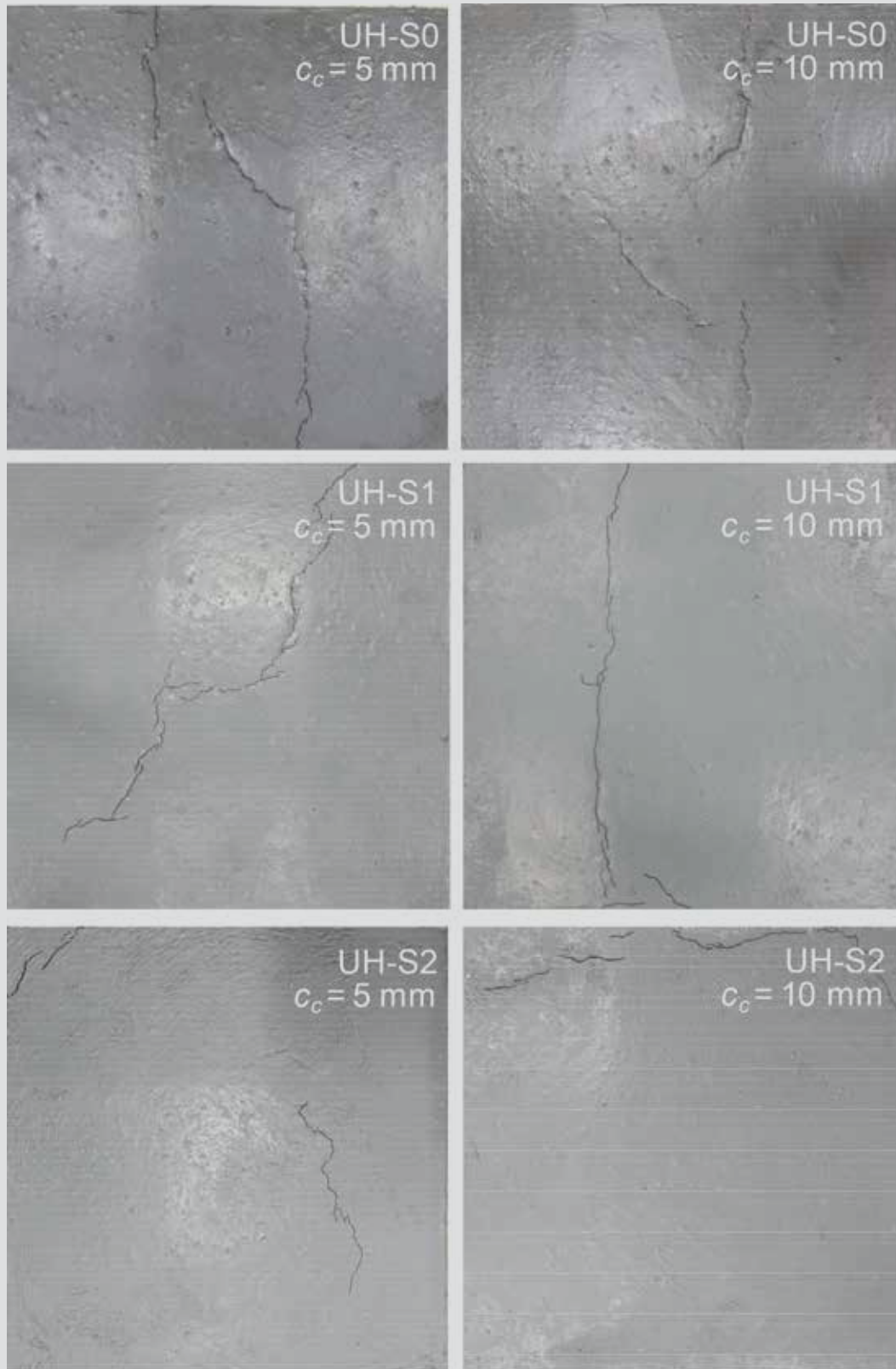


Figure 11. Surface-cracking behaviors with different shrinkage-reducing admixture dosages and cover depths. Note: c_c = concrete cover depth. 1 mm = 0.0394 in.

UHPFRC slabs according to SRA dosage rate and cover depth. Surface cracking occurred mostly in a direction parallel to the longitudinal direction of the upper steel reinforcement due to the settling of the UHPFRC at an

early age.²⁷ However, the specimens with a cover depth of 20 mm (0.79 in.) (approximately 1.3 times larger than the bar diameter) showed no surface cracking during testing regardless of SRA dosage. Therefore, the minimum cover

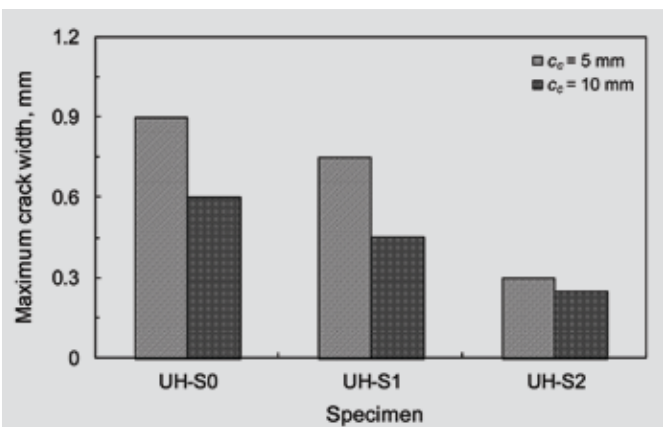


Figure 12. Maximum surface-crack width for ultra-high-performance fiber-reinforced concrete slabs after 30 days. Note: c_c = concrete cover depth. 1 mm = 0.0394 in.

depth for UHPFRC slabs to prevent surface cracking by settling is conservatively suggested to be 1.3 times the diameter of the upper reinforcing bars for applications that include a wide range of steel reinforcing-bar diameters.

Figure 12 exhibits the maximum crack widths of the slabs after 30 days. The maximum crack widths decreased as SRA dosage and cover depth increased. For example, the maximum crack width of UH-S2, with a cover depth of 5 mm (0.2 in.), was found to be 0.30 mm (0.012 in.), approximately 60% and 67% less than those of UH-S1 and UH-S0, respectively. Therefore, it was concluded that the use of a SRA and the increase of cover depth are effective in improving the surface-cracking resistance of UHPFRC slabs.

Conclusion

In this study, the effects of SRA dosage and cover depth on the shrinkage and surface-cracking behaviors of UHPFRC slabs were investigated. From the previous discussions, the following conclusions are drawn:

- Initial and final setting times were delayed as a function of SRA dosage. In addition, mass loss and maximum rate of evaporation decreased as SRA dosage increased up to 2% because of the increase of the pore solution's viscosity.
- The shrinkage strain of UHPFRC slabs without steel reinforcement decreased by adding SRA, and the reduction in shrinkage strain increased with SRA dosage. Shrinkage strain significantly decreased as depth increased from the top surface to a depth of 18 mm (0.71 in.). For lower depths, shrinkage strain gradually decreased with depth due to the extremely densified microstructure of UHPFRC.
- Early-age residual strains in steel reinforcement (at one day) were almost three times less than early-age shrinkage strains without reinforcement, owing to

the low elastic modulus of UHPFRC at early age. For this reason, the 30-day residual strains significantly decreased compared with the shrinkage strains without reinforcement. In addition, the degree of restraint decreased as cover depth increased for all test series. Thus, a greater cover depth was favorable because it caused a lower degree of restraint and cracking potential in UHPFRC slabs by the restraint of shrinkage.

- The slabs with cover depths less than 20 mm (0.79 in.) (1.3 times the reinforcing-bar diameter) yielded surface cracking parallel to the longitudinal direction of the upper steel reinforcing bars from the settlement of UHPFRC. Therefore, the minimum cover depth for the UHPFRC slabs is conservatively suggested as 1.3 times the reinforcing-bar diameter in order to prevent surface cracking. In addition, the maximum surface-crack width decreased as SRA dosage and cover depth increased. Accordingly, a SRA and greater cover depth were useful for improving the surface-cracking resistance of UHPFRC slabs.

Acknowledgments

This research was supported by a grant (13SCIPA01) from the Smart Civil Infrastructure Research Program funded by the Ministry of Land, Infrastructure and Transport (MOLIT) of the Korean government and the Korea Agency for Infrastructure Technology Advancement (KAIA).

References

1. Richard, P., and M. Cheyrezy. 1995. "Composition of Reactive Powder Concretes." *Cement and Concrete Research* 25 (7): 1501–1511.
2. Kobler, M., and W. Sobek. 2008. "The Introduction of High Forces into Tine-Walled UHPC Elements by the Use of Implants." In *Proceedings of the Second International Symposium on Ultra High Performance Concrete, Kassel, Germany, March 05–07, 2008*, 683–690. Kassel, Germany: Kassel University Press.
3. Perry, V., and G. Weiss. 2009. "Innovative Field Cast UHPC Joints for Precast Bridge Decks—Design, Prototype Testing and Projects." In *Proceedings of the International Workshop on Ultra High Performance Fibre Reinforced Concrete—Designing and Building with UHPFRC: State of the Art Development*, 421–436. Marseille, France.
4. Kim, Y. J., S. Y. Park, J. S. Park, and B. S. Kim. 2013. "State-of-the-Art of UHPC Applications in the World." *Journal of Korean Society of Civil Engineering* 61 (2): 39–50.

5. Yoo, D. Y., K. Y. Kwon, J. J. Park, and Y. S. Yoon. 2015. "Local Bond-Slip Response of GFRP Rebar in Ultra-High-Performance Fiber-Reinforced Concrete." *Composite Structures*, no. 120: 53–64.
6. Yoo, D. Y., J. J. Park, S. W. Kim, and Y. S. Yoon. 2014. "Influence of Reinforcing Bar Type on Autogenous Shrinkage Stress and Bond Behavior of Ultra High Performance Fiber Reinforced Concrete." *Cement and Concrete Composites*, no. 48: 150–161.
7. JSCE (Japan Society of Civil Engineers). 2004. Recommendations for Design and Construction of Ultra-High Strength Fiber Reinforced Concrete Structures (Draft). Tokyo, Japan: JSCE.
8. Habel, K., J. P. Charron, E. Denarie, and E. Bruhwiler. 2006. "Autogenous Deformations and Viscoelasticity of UHPFRC in Structures. Part 1: Experimental Results." *Magazine of Concrete Research* 58 (3): 135–145.
9. Park, J. J., D. Y. Yoo, S. W. Kim, and Y. S. Yoon. 2013. "Drying Shrinkage Cracking Characteristics of Ultra-High-Performance Fibre Reinforced Concrete with Expansive and Shrinkage Reducing Agents." *Magazine of Concrete Research* 65 (4): 248–256.
10. Yoo, D. Y., J. J. Park, S. W. Kim, and Y. S. Yoon. 2014. "Influence of Ring Size on the Restrained Shrinkage Behavior of Ultra High Performance Fiber Reinforced Concrete." *Materials and Structures* 47 (7): 1161–1174.
11. Yoo, D. Y., K. H. Min, J. H. Lee, and Y. S. Yoon. 2014. "Shrinkage and Cracking of Restrained Ultra-High-Performance Fiber-Reinforced Concrete Slabs at Early Age." *Construction and Building Materials*, no. 73: 357–365.
12. KSA (Korea Standard Association). 2009. *Standard Test Method for Dry Shrinkage Crack in Concrete*. KS F 2595. Seoul, Korea: KSA.
13. Bentz, D. P. 2008. "A Review of Early-Age Properties of Cement Based Materials." *Cement and Concrete Research* 38 (2): 196–204.
14. ASTM Subcommittee C01.22. 2007. *Standard Test Method for Flow of Hydraulic Cement Mortar*. ASTM C1437. West Conshohocken, PA: ASTM International.
15. Saliba, J., E. Rozière, F. Grondin, and A. Loukili. 2011. "Influence of Shrinkage-Reducing Admixtures on Plastic and Long-Term Shrinkage." *Cement and Concrete Composites* 33 (2): 209–217.
16. Yoo, D. Y., S. T. Kang, J. H. Lee, and Y. S. Yoon. 2013. "Effect of Shrinkage Reducing Admixture on Tensile and Flexural Behaviors of UHPFRC Considering Fiber Distribution Characteristics." *Cement and Concrete Research*, no. 54: 180–190.
17. ASTM Subcommittee C09.23. 2008. *Standard Test Method for Time of Setting of Concrete Mixtures by Penetration Resistance*. ASTM C403/C403M. West Conshohocken, PA: ASTM International.
18. Yoo, D. Y., J. J. Park, S. W. Kim, and Y. S. Yoon. 2013. "Early Age Setting, Shrinkage and Tensile Characteristics of Ultra High Performance Fiber Reinforced Concrete." *Construction and Building Materials*, no. 41: 427–438.
19. Pelisser, F., A. B. S. S. Neto, H. L. L. Rovere, and R. C. A. Pinto. 2010. "Effect of the Addition of Synthetic Fibers to Concrete Thin Slabs on Plastic Shrinkage Cracking." *Construction and Building Materials* 24 (11): 2171–2176.
20. Yoo, D. Y., K. Y. Kwon, J. M. Yang, and Y. S. Yoon. 2015. "Effect of Cover Depth and Rebar Diameter on Shrinkage Behavior of Ultra-High-Performance Fiber-Reinforced Concrete Slabs." *Structural Engineering and Mechanics*, under review.
21. Brooks, J. J., M. A. M. Johari, and M. Mazloom. 2000. "Effect of Admixtures on the Setting Times of High-Strength Concrete." *Cement and Concrete Composites* 22 (4): 293–301.
22. Mora-Ruacho, J., R. Gettu, and A. Aguado. 2009. "Influence of Shrinkage-Reducing Admixtures on the Reduction of Plastic Shrinkage Cracking in Concrete." *Cement and Concrete Research* 39 (3): 141–146.
23. Bentz, D. P. 2006. "Influence of Shrinkage-Reducing Admixtures on Early-Age Properties of Cement Pastes." *Journal of Advanced Concrete Technology* 4 (3): 423–429.
24. Chen, H. L. R., and J. H. Choi. 2011. "Analysis of Shrinkage and Thermal Stresses in Concrete Slabs Reinforced with GFRP Rebars." *Journal of Materials in Civil Engineering* 23 (5): 612–627.
25. Yoo, D. Y., N. Banthia, and Y. S. Yoon. 2015. "Effectiveness of Shrinkage-Reducing Admixture in Reducing Autogenous Shrinkage Stress of Ultra-High-Performance Fiber-Reinforced Concrete." *Cement and Concrete Composites*, no. 64: 27–36.
26. Hossain, A. B., and W. J. Weiss. 2004. "Assessing Residual Stress Development and Stress Relaxation in Restrained Concrete Ring Specimens." *Cement and Concrete Composites* 26 (5): 531–540.
27. Kyle, N. L. 2001. "Subsidence Cracking of Concrete

Over Steel Reinforcement Bar in Bridge Decks.” MS thesis, Virginia Polytechnic Institute and State University, Blacksburg, VA.

Notation

c_c = concrete cover depth

d_f = diameter of fiber

E_f = elastic modulus of fiber

f_t = tensile strength of fiber

h = depth of concrete slab

L_f = length of fiber

V_f = volume fraction of fiber

ε_s = strain in steel reinforcement

ε_{sh} = shrinkage strain of concrete without reinforcement

ψ = degree of restraint

About the authors



Doo-Yeol Yoo, PhD, is a postdoctoral fellow in the Department of Civil Engineering at the University of British Columbia in Vancouver, BC, Canada. He received his PhD from Korea University in Seoul, South Korea. His research interests include

the design, analysis, and modeling of ultra-high-performance fiber-reinforced concrete.



Nemkumar Banthia, PhD, PEng, is a distinguished professor and senior Canada research chair in infrastructure rehabilitation in the Department of Civil Engineering at the University of British Columbia. He holds five patents and has published more

than 400 refereed papers. He serves as the editor-in-chief of the *Journal of Cement and Concrete Composites*. He is a fellow of the American Concrete Institute, Canadian Society for Civil Engineering, Indian Concrete Institute, Canadian Academy of Engineering, and Royal Society of Canada.



Young-Soo Yoon, PhD, is a professor in the School of Civil, Environmental, and Architectural Engineering at Korea University. He received his PhD from McGill University in Montreal, QC, Canada. His research interests include shear behavior,

high-performance concrete, ultra-high-strength concrete, and the structural use of fibers.

Abstract

This study investigates the effects of shrinkage-reducing admixture (SRA) and cover depth on the shrinkage and surface-cracking behaviors of ultra-high-performance fiber-reinforced concrete (UHPFRC) slabs. Three different SRA-to-cement weight ratios of 0%, 1%, and 2%, and three different cover depths, 5, 10, and 20 mm (0.2, 0.4, and 0.8 in.), were considered using nine UHPFRC slabs with steel reinforcing bars. Three more unreinforced UHPFRC slabs with three different SRA ratios and four different depths were also fabricated for the comparisons. The use of SRA exhibited better behavior with regard to the decrease of shrinkage, maximum evaporation rate, and maximum surface-crack width. In addition, the application of a larger cover depth was favorable because it caused a lower degree of restraint, leading to a lower cracking potential and a higher surface-cracking resistance. Finally, the minimum required cover depth of the UHPFRC slab is suggested to be 1.3 times larger than the diameter of the upper steel reinforcing bar in order to prevent surface cracking.

Keywords

Cover depth; degree of restraint; shrinkage-reducing admixture; slab; surface cracking; ultra-high-performance fiber-reinforced concrete.

Review policy

This paper was reviewed in accordance with the Precast/Prestressed Concrete Institute's peer-review process.

Reader comments

Please address reader comments to journal@pci.org or Precast/Prestressed Concrete Institute, c/o PCI Journal, 200 W. Adams St., Suite 2100, Chicago, IL 60606. ■